LANGMUIR

pubs.acs.org/Langmuir Article

Solute Stabilization Effects of Nanoparticles Containing Boronic Acids in the Absence of Binding Pairs

Jeonghun Lee, Karla Cureño Hernandez, Sunghoon Kim, and Margarita Herrera-Alonso*

Cite This: *Langmuir* 2023, 39, 15328−15337 Read Online

ACCESS | Metrics & More | Article Recommendations | Supporting Information

ABSTRACT: Boronic acids are widely used in materials science because of their ability to reversibly bind with diol and catechol moieties through dynamic covalent interactions in a pH- and oxidative-dependent manner. Considerably fewer studies focus on property modulation of boronic acid−based materials in the absence of a biding pair. Herein, we discuss the effects of the boronic acid-containing polymer block length on solute release kinetics from nanoparticles in a stimuli-responsive manner for on-demand delivery. In this study, ABC-type linear amphiphiles of poly(D,L-lactide) and poly(2-methacryloyloxyethyl phosphorylcholine) containing a middle block functionalized with 3-aminophenylboronic acid were synthesized by a combination of ring-opening and controlled free radical polymerizations. Nile red-loaded nanoparticles were self-assembled using a multi-inlet vortex mixer in a well-controlled manner. Release was evaluated at pH above and below the pK_a of the boronic acid and in the presence of hydrogen peroxide. Our results show that release kinetics from nanoparticles incorporating a boronic acid-functionalized interlayer were slower than those without it, and the rate could be modulated according to pH and oxidative conditions. These effects can be attributed to several factors, including the hydrophobicity of the boronic acid block as well as hydrogen bonding interactions existing between locally confined boronic acids. While boronic acids are generally utilized as boronic/boronate esters, their stabilizing effects in the absence of appropriate binding pairs are relevant and should be considered in the design of boronic acid-based technologies.

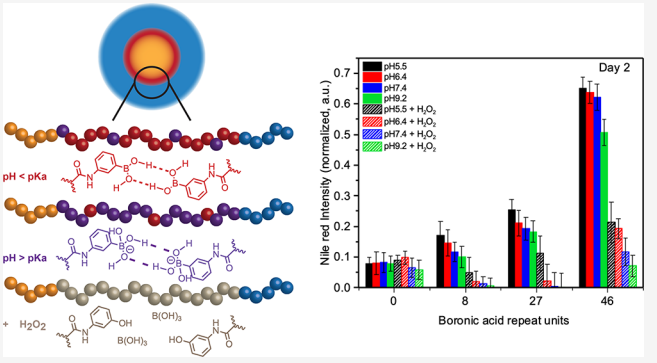

INTRODUCTION

Phenylboronic acids are important structural motifs for the construction of functional polymers and supramolecular networks, with applications in sensing, separation, responsive biomaterials, and drug delivery.[1−8] Their widespread interest is 2-fold. First is their ability to reversibly bind with vicinal diols. The formation of boronic esters (neutral) or boronate esters (anionic) is not only pH-responsive but also sensitive to hydrolysis or competitive binding interactions with other diol-containing molecules. Other nucleophilic compounds with good binding affinity to boronic acids include dicarboxylic acids and alpha-hydroxy-carboxylic acids, but are far less reported than diol- or catechol-based systems.[3] In multivalent forms, phenylboronic acid- and diol-containing polymers yield cross-linked networks, widely used the synthesis of self-healing polymers and environmentally responsive hydrogels,[9−16] and for the development of smart materials.[17,18] A second important attribute of phenylboronic acids is their susceptibility toward H_2O_2, yielding phenol and boric acids as oxidation products. The overproduction of reactive oxygen species, in particular, H_2O_2, is often observed in degenerative or metabolic diseases and inflamed tissue and is known to modulate cancer metastasis. In this sense, boronic acid-containing polymers have been designed to enable H_2O_2 detection, as theranostic agents for thrombosed vessels, and to induce triggered degradation in H_2O_2-rich media.[19−22]

In the contest of drug carriers, boronic acids have been used as polymeric substrates for the encapsulation and environmentally triggered release of diol/catechol-containing payloads,[23,24] as targeting motifs for bacterial detection or selective binding to sialylated epitopes on cancer cells,[25−30] and in micellar stabilization.[7,31−37] Stabilization, generally achieved through the formation of permanent (nondegradable) covalent bonds, is intended to prevent dissociation under high dilution and modulate drug release kinetics.[33,38−44] More recently, the emphasis toward reversible cross-linking has triggered incorporation of functionalities amenable to dynamic-covalent interactions due to their inherent reversibility but also their stimuli-responsiveness. The choice of the dynamic-covalent interaction is crucial in these applications, as the type of bond

Received: July 31, 2023
Revised: September 19, 2023
Published: October 16, 2023

https://doi.org/10.1021/acs.langmuir.3c02181
Langmuir 2023, 39, 15328−15337

Table 1. Characterization of the ZP and ZPB Block Copolymers Studied Herein

polymer		PAPBMA conv. (%)[a]	PAPBMA DP[a]	PMPC conv. (%)[a]	PMPC DP[a]	M_n, theory (Da)[a]	C_{CMC} (μg/mL)[b]
ZP1	PLA_{68}-*b*-$PMPC_{94}$	0	0	94.1	94	38,091	3.96
ZPB1	PLA_{68}-*b*-$PAPBMA_8$-*b*-$PMPC_{98}$	82.5	8	97.9	98	40,784	4.06
ZPB2	PLA_{68}-*b*-$PAPBMA_{27}$-*b*-$PMPC_{95}$	91.7	27	95.1	95	43,490	4.26
ZPB3	PLA_{68}-*b*-$PAPBMA_{46}$-*b*-$PMPC_{97}$	92.3	46	97.3	97	47,672	4.74
ZP2	PLA_{79}-*b*-$PMPC_{94}$	0	0	94.2	94	39,528	3.77
ZP3	PLA_{138}-*b*-$PMPC_{94}$	0	0	94.2	94	48,032	2.39

[a]Determined by ^{1}H NMR. [b]Critical micelle concentration (C_{CMC}) was measured by fluorescence spectroscopy using pyrene as a probe.

will define the kinetic and thermodynamic features of the system. Most dynamic-covalent cross-linked micelles are based on disulfide cross-linking because of its responsiveness toward glutathione. Other examples, of which fewer cases exist, target the use of boronic ester condensation as the cross-linking motif. Noteworthy examples include acid-responsive shell-cross-linked micelles of boronic acid/dextran for the delivery of doxorubicin,[37] boronic acid/mannitol for the delivery of paclitaxel,[45] phenylboronate/gluconamide for pDNA delivery,[46] and phenylboronic acid/dopamine for the delivery of camptothecin.[47]

In the absence of binding pairs, boronic acid−based polymers can still establish noncovalent interactions via hydrogen bonding. Hydrogen bonds are formed through −O···H−O− interaction in homodimers, generally studied for free acids in which the boron atom preserves its trigonal neutral form.[48−50] This secondary interaction of boronic acids has only scarcely been used as a physicochemical property modulator despite its environmental sensitivity. Examples in which property enhancement was attributed to boronic acid hydrogen bonding include the enhanced activation of boronic acid organocatalysts,[51] control of the elastic properties of silicone-boronate polymers,[52] direct supramolecular construction,[53] and the high strength of Pickering emulsions stabilized by boronic acid homopolymers.[54]

Herein we explore the use of boronic acid-containing triblock copolymers to control solute partitioning from nanoparticles in the absence of binding pairs. For this, ABC-type amphiphilic copolymers of poly(D,L-lactide) and poly(2-methacryloyloxyethyl phosphocholine) containing a middle block functionalized with 3-aminophenylboronic acid were used for the formation of Nile red-loaded nanoparticles through self-assembly in a multi-inlet vortex mixer. Solute release kinetics were evaluated under different conditions to establish the role of the boronic acid block length as the determinant of solute release kinetics. We observed a solute stabilization effect from boronic acid-containing copolymers to delay release over a 48 h period, sensitive to block length, system pH, and the presence of H_2O_2.

EXPERIMENTAL SECTION

Materials. All chemical and solvents were commercially available and purchased from Fisher Scientific, TCI, and Sigma-Aldrich unless otherwise noted. 4-Cyano-4-[(dodecylsulfanylthiocarbonyl) sulfanyl]-pentanoic acid (CDTPA) was purchased from Angina Chemical. 2-(Methacryloyloxy)ethyl 2-(trimethylammonio) ethyl phosphate (MPC) and 3-metacrylamidophenylboronic acid (APBMA) were purchased from Ambeed. D,L-Lactide and AIBN were recrystallized from hot methanol and ethyl acetate, respectively. Nanopure water was purified in a Barnstead Nanopure system with a final resistance of 18.2 MΩ. 1,8-Diazabicyclo [5.4.0]undec-7-ene (DBU) was dried over molecular sieves (3 Å) for no less than 12 h.

Synthesis of Poly(D,L-lactide) (PLA). Copolymers based on PLA of three different lengths were used in this study: PLA_{68}, PLA_{79}, and PLA_{138}. To synthesize PLA_{68}, D,L-lactide (5 g, 34.69 mmol) was loaded into a dry Schlenk flask and placed under a high vacuum at 40 °C for 3 h. After backfilling with argon, the monomer was dissolved in ∼10 mL of anhydrous dichloromethane (DCM). Octanol (75.79 μL, 0.48 mmol) and DBU (52.81 μL, 0.35 mmol) were sequentially injected into the flask. Polymerization was conducted at room temperature for 2 h under argon. The reaction was quenched by opening it to atmosphere and on the addition of benzoic acid (211.8 mg, 1.73 mmol). An aliquot of the mixture was taken to calculate monomer conversion. The solution was concentrated with a rotary evaporator and precipitated into cold methanol three times. The resulting polymer was dried under vacuum at room temperature overnight. Yield: 90.2%. Monomer conversion was 94.0%, determined by ^{1}H NMR, and the degree of polymerization of PLA was evaluated by end-group analysis. This procedure was followed for the synthesis of PLA_{79} and PLA_{138} using the following: (a) for PLA_{79}: D,L-lactide (6 g, 41.6 mmol), octanol (59.53 μL, 0.038 mmol), DBU (62.26 μL, 0.42 mmol); (b) for PLA_{138}: D,L-lactide (6 g, 41.6 mmol), octanol (46.77 μL, 0.03 mmol), and DBU (62.26 μL, 0.42 mmol). PLA_{79} yield was 89.3% and monomer conversion was 98.8%, whereas for PLA_{138} these were 84.4 and 98.6%, respectively. ^{1}H NMR of PLA and peak assignments are provided in Figure S1, and chromatograms of all polymers are included in Figure S2.

Synthesis of PLA-macroCTA (PLA-CTA). PLA-CTA was synthesized by DCC/DMAP-mediated coupling of carboxylic acid-CTA with PLA. The molar ratio of PLA to CDTPA, *N*,*N*′-dicyclohexylcarbodiimide (DCC), and dimethylpyridine (DMAP) was 1:3:3:0.3, respectively. For example, to synthesize PLA_{68}-CTA, PLA (3 g, 0.30 mmol), CDTPA (365.82 mg, 0.91 mmol), DCC (186.99 mg, 0.91 mmol), and DMAP (11.07 mg, 0.091 mmol) were dissolved in 30 mL of anhydrous THF, and the reaction was carried out at 40 °C for 18 h with continuous stirring. The resulting mixture was filtered to remove salts, and the filtrate was concentrated by rotary evaporation. The concentrated mixture was precipitated into cold methanol three times. The resulting materials were dried under a vacuum at room temperature overnight. Yield: 97.5%. ^{1}H NMR of PLA-CTA is provided in Figure S3.

Synthesis of PLA-*b*-PMPC (ZP1, ZP2, ZP3). To synthesize PLA_{68}-*b*-$PMPC_{94}$ (ZP1), PLA_{68}-CTA (1 g, 0.097 mmol) and MPC (3.14 g, 10.64 mmol) were added to a dry Schlenk flask and dissolved in 17 mL of methanol and *N*,*N*′-dimethylformamide (DMF) (50% v/v). AIBN (3.18 mg, 0.019 mmol) was dissolved in DMF (0.74 mL). The AIBN solution was injected into a Schlenk flask and bubbled with argon at room temperature for 30 min. Polymerization was conducted at 65 °C for 18 h. The reaction was stopped by submerging the flask in an ice bath and opening it to atmosphere. An aliquot was taken to calculate the monomer conversion. Yield: 92.0%. This procedure was followed for the synthesis of diblock copolymers of PMPC and PLA_{79} or PLA_{138}. For PLA_{79}-*b*-$PMPC_{94}$ (ZP2): PLA_{79}-CTA (0.4 g, 0.03 mmol), MPC (1.0 g, 3.4 mmol), AIBN (1.2 mg, 0.01 mmol), methanol/DMF (8.49 mL, 50% v/v); yield: 85.0%. For PLA_{138}-*b*-$PMPC_{94}$ (ZP3): PLA_{138}-CTA (0.6 g, 0.03 mmol), MPC (867 mg, 2.94 mmol), AIBN (0.96 mg, 0.01 mmol), and methanol/DMF (7.34 mL, 50% v/v); yield 87.0%. Conversions were estimated by ^{1}H NMR

https://doi.org/10.1021/acs.langmuir.3c02181
Langmuir 2023, 39, 15328−15337

as shown in Table 1. ^{1}H NMR peak assignments of PLA-*b*-PMPC are provided in Figure S4, and the GPC data is included in Figure S2.

Synthesis of PLA-*b*-PAPBMA. PLA_{68}-CTA (1.0 g, 0.10 mmol) and APBMA (198.37 mg, 0.97 mmol) were placed in a Schlenk flask and dissolved in DMF (1.53 mL) and DIW (80.6 μL) with vigorous stirring. AIBN (2.22 mg, 0.01 mmol) was dissolved in DMF (500 μL) and added to the flask. The mixture was bubbled with argon for 30 min. After bubbling, the flask was submerged in an oil bath at 70 °C to conduct polymerization for 18 h under argon. The polymerization was quenched by removing the rubber septum, bubbling air into the flask, and submerging it in an ice bath. The degree of polymerization of APBMA was 8 repeat units, determined by ^{1}H NMR. The synthesis of diblock macro-CTAs with longer APBMA segments was carried out using the same protocol and the same amounts of PLA_{68}-CTA and AIBN as mentioned above, but with the following changes: (a) for the synthesis of PLA_{68}-*b*-$PAPBMA_{27}$, APBMA (595.1 mg, 2.90 mmol), DMF (4.5 mL), and DIW (242 μL) were used; (b) for the synthesis of PLA_{68}-*b*-$PAPBMA_{46}$, APBMA (991.83 mg, 4.84 mmol), DMF (7.6 mL), and DIW (403.1 μL) were used. Monomer conversion was determined by the ^{1}H NMR of an aliquot. The resulting solution was concentrated using a rotary evaporator and then precipitated into cold diethyl ether three times. The final product was collected by vacuum filtration after precipitation and dried under vacuum overnight. Yield: 91.4, 87.2, and 86.7%, respectively. Monomer conversion and the degree of polymerization are summarized in Table 1. ^{1}H NMR peak assignments of PLA-*b*-PAPBMA are shown in Figure S5.

Synthesis of PLA-*b*-PAPBMA-*b*-PMPC (ZPB1, ZPB2, ZPB3). For the synthesis of PLA_{68}-*b*-$PAPBMA_8$-*b*-$PMPC_{98}$ (ZPB1), PLA_{68}-*b*-$PAPBMA_8$ macro-CTA (0.5 g, 0.042 mmol), MPC (1.23 g, 4.18 mmol), and AIBN (1.37 mg, 0.008 mmol) were loaded into a Schlenk flask. A solvent combination of DMF (4.70 mL, 45% v/v), MeOH (5.22 mL, 50% v/v), and deionized water (DIW, 0.52 mL, 5% v/v) was injected into the flask and mixed with the reagents under stirring. The solution was bubbled with argon for 30 min at room temperature, and the flask was then immersed in an oil bath at 65 °C for 18 h. The reaction was quenched by removing the rubber septum and cooling the flask in an ice bath. The syntheses of triblock copolymers from PLA_{68}-*b*-$PAPBMA_{27}$ and PLA_{68}-*b*-$PAPBMA_{46}$ macro-CTAs were conducted following the same procedure as described above, with the following amounts of reagents: (a) PLA_{68}-*b*-$PAPBMA_{27}$ (0.6 g, 0.038 mmol), MPC (1.12 g, 3.78 mmol), AIBN (1.24 mg, 0.008 mmol), DMF (4.253 mL, 45% v/v), MeOH (4.72 mL, 50% v/v), DIW (0.47 mL, 5% v/v); (b) PLA_{68}-*b*-$PAPBMA_{46}$ (1.0 g, 0.051 mmol), MPC (1.48 g, 5.06 mmol), AIBN (1.66 mg, 0.01 mmol), DMF (5.69 mL, 45% v/v), MeOH (6.32 mL, 50% v/v), and DIW (0.63 mL, 5% v/v). In all cases, aliquots were collected to calculate MPC conversion by ^{1}H NMR. The resulting solutions were directly loaded into dialysis bags (6−8 kDa MWCO, SpectraPor) and dialyzed against a mixture of methanol/acetone (50% v/v). The solvent mixture was replenished every 3 h and changed to Nanopure water after 24 h. Polymers were further dialyzed against Nanopure water for another 24 h and lyophilized. Yields: 85.6, 81.2, and 80.2%, respectively. A summary of the characterization of these polymers is presented in Table 1. ^{1}H NMR peak assignments of triblocks are shown in Figure S6.

Critical Micelle Concentration. Critical micelle concentrations (C_{CMC}) of polymers were determined by fluorescence spectroscopy using pyrene as a probe. First, a pyrene stock solution was prepared at a concentration of 1.8×10^{-4} M in acetone. Fifteen μL of this stock solution was added to a 5 mL scintillation vial and the solvent was allowed to evaporate completely prior to the addition of 50 μL of a solution of varying concentration of polymer in acetone/methanol (50% v/v). Nanopure water (3 mL) was then added dropwise, and the samples were stirred with a vortex mixer for 1 min. The final concentration of polymer ranged from 0.05 to 0.5 mg/mL. The solvent was allowed to evaporate at room temperature and the samples were equilibrated for 18 h at room temperature under a dark fume hood prior to measurements. Pyrene excitation was recorded from 300 to 360 nm with an emission wavelength of 390 nm. The intensity ratio from fluorescence spectroscopy signals at 336 and 334 nm (I_{336}/I_{334}) was read and plotted as a function of polymer concentration. C_{CMC} was estimated from the intersection between curve tangents at low and high concentration (Figure S7).

Nanoparticle Formation from a Multi-Inlet Vortex Mixer (MIVM). Nanoparticles were prepared by triggering a large and rapid change in the solvent quality inside a four-stream vortex mixer (MIVM). First, the polymer stock solution (10 mg/mL in methanol/dimethylformamide, 50% v/v) was prepared at room temperature and filtered through a 0.45 μm hydrophilic PVDF syringe filter (Millipore). This solution was loaded into a 10 mL syringe (Hamilton) and mounted on a syringe pump (Harvard Apparatus). Nanopure water was loaded into three 50 mL syringes (Hamilton), which were mounted on a separate pump (Harvard Apparatus). Organic and aqueous lines were then carefully connected to the four-stream mixer. The MeOH/DMF:water volumetric ratio used was 1:9, with mixing speeds of 12 and 108 mL/min for the organic and water streams, respectively. Samples were collected 6 s after the start of the mixing process to ensure steady operation of the mixer. Nanoparticle suspensions were dialyzed (6−8 kDa MWCO, SpectraPor) against Nanopure water for 12 h to eliminate the organic solvent. Water was replenished six times during the dialysis process. Nanoparticle suspensions were stored in clean vials for further characterization.

Nile Red-Loaded Nanoparticles from MIVM. Nile red (NR)-loaded nanoparticles were prepared by using the MIVM, as described above. In this case, NR (0.1% w/w_p) and the polymer in question were dissolved together in MeOH/DMF (50% v/v) at room temperature. This solution was loaded into a 10 mL syringe (Hamilton). Subsequent steps were followed, as described above. Nanoparticle suspensions were stored in clean vials for further characterization by DLS and TEM (Figure S8).

Alizarin Red Fluorescence Studies. Alizarin red S (ARS) is a catechol dye that binds to boronic acids, resulting in a significant change in the ARS fluorescence intensity. ARS solutions were prepared at a concentration of 1.8×10^{-6} M in phosphate buffered saline (PBS) at pH 7.4. Nanoparticle solution was prepared at a concentration of 1 mg/mL in PBS. 1.0 mL of ARS solution and 1.0 mL of nanoparticle solution were mixed in a 5 mL vial and allowed to reach equilibrium for 30 min. Fluorescence intensity was recorded at 575 nm with an excitation wavelength of 470 nm. All experiments were repeated in triplicate.

Nile Red Release Profile. Nile red (NR) release was examined for the nanoparticles from ZP1 and ZPB1−3. For these experiments, 5 mL of NR-encapsulated nanoparticle suspensions was loaded into dialysis bags (6−8 kDa MWCO, SpectraPor) and dialyzed against buffers prepared with different pH values (5.5, 6.4, 7.4, and 9.2). The release medium was stirred at 500 rpm. Aliquots (2 mL) were taken at predetermined time points from the suspension for measurement and reintroduced to the dialysis bag after measurement to maintain a constant suspension volume. NR fluorescence intensity was measured at 615 nm with an excitation wavelength of 535 nm. Values are reported as the averages of three independent replicates and plotted as functions of time. To evaluate NR release under oxidative conditions, hydrogen peroxide was added to different pH buffers to reach the concentration of 1 mM and the same procedure as described above was followed. All experiments were repeated in triplicate.

PAPBMA Solubility in Nanoparticles. Boronic acids ionize upon exposure to an environment pK_a < pH, resulting in an anionic tetrahedral form with an enhanced affinity toward water. To examine the solubility of the PAPBMA block, the pH of D_2O was adjusted with either TEA or PBS to achieve a pH of 9.2 or 7.4, respectively. Lyophilized nanoparticles were dispersed in each solution for ^{1}H NMR acquisition (Figure S9).

Nanoparticle Stability. Nanoparticles were prepared by MIVM and dialyzed against Nanopure water for 12 h. The medium was then changed to buffered solutions to achieve suspensions at pH values of 5.5, 6.4, 7.4, and 9.2. Nanoparticle size was measured at predetermined time points for each medium and plotted as the average particle size over time.

https://doi.org/10.1021/acs.langmuir.3c02181
Langmuir 2023, 39, 15328−15337

Scheme 1. Synthesis of Zwitterionic Di- and Triblock Copolymers by a Combination of Ring-Opening and Reversible Addition−Fragmentation Chain-Transfer Polymerizations[a]

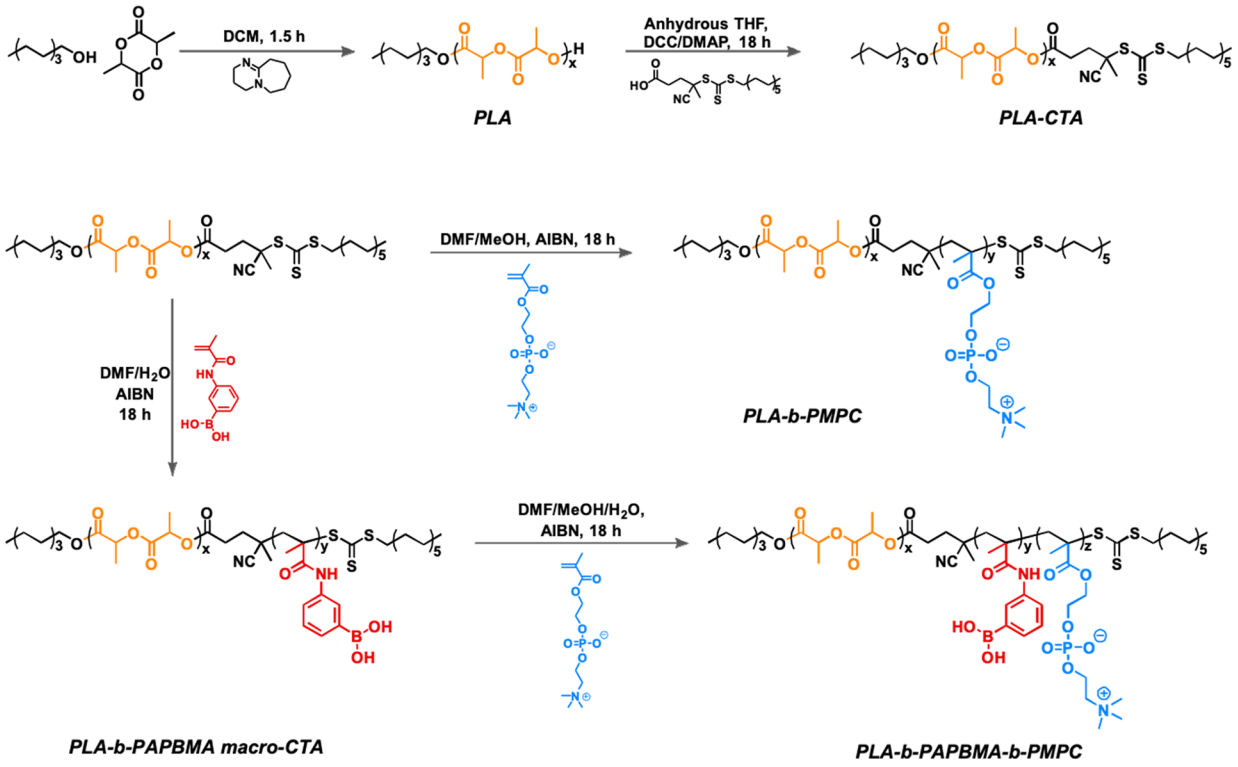

[a]The triblock copolymers contain a middle block functionalized with an aminophenylboronic acid moiety.

RESULTS AND DISCUSSION

Nanoparticle Characterization. Zwitterionic amphiphiles were synthesized by a combination of ring-opening polymerization (ROP) of D,L-lactide and the sequential reversible addition−fragmentation chain-transfer (RAFT) polymerization of 3-methacrylamidophenylboronic acid (APBMA) and 2-methacryloyloxyethyl phosphorylcholine (MPC) (Scheme 1). First, D,L-lactide was polymerized by ROP with a conversion of 97%. The terminal hydroxyl was used to conjugate a chain transfer agent for RAFT. This was achieved by DCC/DMAP coupling with high efficiency, as assessed by ^{1}H NMR (quantitive conversion). Then, different block lengths of APBMA were polymerized by controlling the feed ratio of monomer to macro-chain transfer agent. Successful polymerization of APBMA was confirmed by ^{1}H NMR (Figures S1, S3−S6), yielding boronic acid-containing block lengths between 0 and 46 repeat units. Polymerization of the zwitterionic block was carried out in a cosolvent system of methanol/dimethylformamide (50% v/v) due to the differences in solubility between poly(D,L-lactide) and the zwitterionic monomer (eventually, polymer). This difference in solubilities of polyesters and PMPC had previously been observed for copolymers of PMPC-*b*-PCL and PMPC-*b*-PLA.[55−60] MPC was polymerized to yield a block length of approximately 95 repeat units.

A summary of the copolymer studied is provided in Table 1, and details regarding their characterization are included in the Supporting Information. GPC analysis was carried out exclusively for PLA and PLA-*b*-PMPC (Figure S2) because copolymers containing the boronic acid monomer were observed to interact with the columns. The results showed both samples had low polydispersities, and in the case of the PLA-*b*-PMPC diblock copolymer, no macroinitiator peak was observed, confirming the effectiveness of conjugation with the CTA (4-cyano-4-[(dodecylsulfanylthiocarbonyl)sulfanyl]-pentanoic acid). For further reference, zwitterionic diblock copolymers of PLA-*b*-PMPC are denoted as ZP1, ZP2, and ZP3 with increasing block length of PLA, whereas triblock copolymers of PLA-*b*-PAPBMA-*b*-PMPC are identified in terms of increasing length of the boronic acid segment as ZPB1, ZPB2, and ZPB3.

Critical micelle concentrations (C_{CMC}) of all copolymers were measured in Nanopure water (pH ∼ 6) using pyrene as the fluorescent probe. As shown in Table 1, we observed a small but consistent increase in C_{CMC} of PLA-*b*-PAPBMA-*b*-PMPC triblocks with PAPBMA block length, ranging from 4.06 to 4.74 μg/mL. This trend was unexpected since pH ∼ 6 is lower than the pK_a of APBMA (pK_a ∼ 8.2), hence the boronic acid exists primarily in its neutral hydrophobic form with only a few moieties present as anionic (hydrophilic) boronates. Conversely to this trend, PLA-*b*-PMPC diblocks shows an expected decrease in C_{CMC} with increasing PLA block length, from 3.96 to 2.39 μg/mL. Comparing di- and triblocks with similar number of non-PMPC repeats suggests that the strongest contributor to the hydrophobic character of these polymers is PLA. This can be observed when comparing the C_{CMC} of ZPB1 with ZP2 (with 79 and 76 non-PMPC repeats, respectively), or ZPB3 with ZP3 (with 114 and 138 non-PMPC repeats, respectively); in both cases, replacement of PAPBMA for PLA resulted in a decrease in C_{CMC}.

Di- and triblock copolymers were self-assembled by imposing a large and rapid change in solvent quality inside a multi-inlet vortex mixer (MIVM), schematically shown in

https://doi.org/10.1021/acs.langmuir.3c02181
Langmuir 2023, 39, 15328−15337

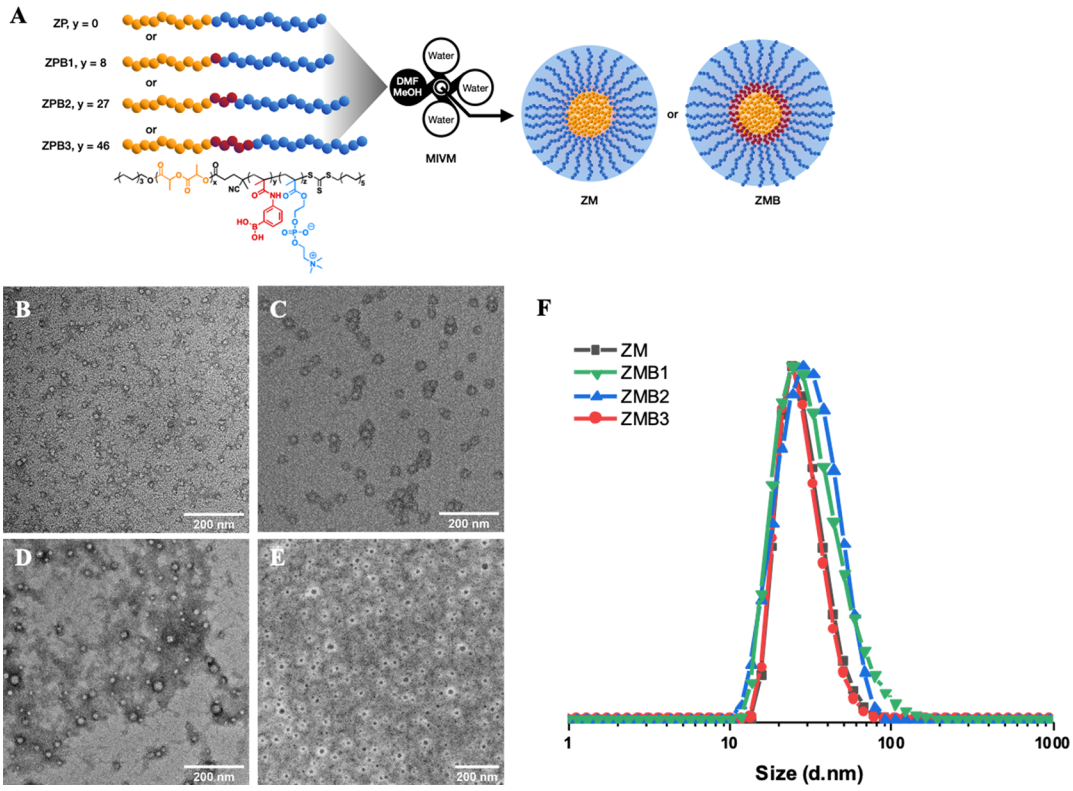

Figure 1. (A) Schematic of the self-assembly of amphiphiles into nanoparticles using a multi-inlet vortex mixer (MIVM), triggered by a rapid change in solvent quality. (B–E) TEM images of nanoparticles with spherical morphologies from ZM (B), ZMB1 (C), ZMB2 (D), and ZMB3 (E). In all cases, scale bars correspond to 200 nm. (F) Size distributions of nanoparticles measured by dynamic light scattering, showing relatively narrow size distributions regardless of the boronic acid block length.

Table 2. Dynamic Light Scattering Characterization of Nanoparticles from Diblock and Triblock Copolymers

		unloaded NPs		Nile red-loaded NPs	
	polymer	D_h (nm)	PDI	D_h (nm)	PDI
ZM	PLA_{68}-*b*-$PMPC_{94}$	38.2	0.13	39.2	0.11
ZMB1	PLA_{68}-*b*-$PAPBMA_{8}$-*b*-$PMPC_{98}$	47.2	0.22	48.1	0.11
ZMB2	PLA_{68}-*b*-$PAPBMA_{27}$-*b*-$PMPC_{95}$	39.7	0.23	40.1	0.13
ZMB3	PLA_{68}-*b*-$PAPBMA_{46}$-*b*-$PMPC_{97}$	35.5	0.19	37.7	0.13

Figure 1A. In this process, the mixing velocity, solvent:non-solvent ratio, and polymer concentration contribute to nanoparticle size and size distribution. Self-assembly was carried out under conditions of high supersaturation (>100) with the copolymer dissolved in an organic, water-miscible solvent—in this case, DMF/MeOH 50% v/v—and mixed against water to yield nanoparticle suspensions of 1 mg/mL. Spherical nanoparticles were obtained in all cases, as verified by transmission electron microscopy (Figure 1B–E), and narrow particle size distributions with an average hydrodynamic diameter (D_h) of ∼40 nm were measured by dynamic light scattering (Figure 1F and Table 2). The smallest nanoparticles, with the narrowest polydispersity, corresponded to those from the diblock (D_h ∼ 38 nm). This size is consistent with nanoparticles from PLA_{87}-*b*-PEG_{75} (D_h = 24 nm), self-assembled by the same process and mixer as that described herein.[61] The difference between these two sets of nanoparticles could be attributed to a difference in the length of the hydrophobic block (68 vs 87 repeat units) and to the fact that, for the same number of repeat units, PMPC layers have been reported to be thicker than their PEG analogs.[62] On the other hand, nanoparticles from triblocks showed a consistent decrease in diameter with PAPBMA length. We attribute this behavior to intra- and intermolecular noncovalent interactions between boronic acids, similar to shell clicked-cross-linked nanoparticles where a decrease in particle size resulted from an increase in the degree of cross-linking.[63] Nile red was loaded in the core of nanoparticles from diblock or triblock copolymers by hydrophobic interaction. Loaded nanoparticles showed the same behavior as those described above, exhibiting slightly larger sizes and lower polydispersities than their unloaded analogs.

The solubility of the boronic acid block was evaluated by ^{1}H NMR of nanoparticles in D_2O at pHs above and below the pK_a of the boronic acid (pK_a ∼ 8.2). As shown in Figure 2, the only clearly observable signals at pH below the pK_a of APBMA corresponded to those of PMPC; PLA is unobservable because of its insolubility in water. Under these conditions (pH 5.5 and 7.4), APBMA is primarily present in the trigonal (neutral) state, exhibiting limited solubility in the aqueous environment. At pH 9.2, the boronic acid is present in the tetrahedral anionic state with enhanced solubility, as evidenced by the characteristic signals of phenyl boronic acid between 6.75 and 7.25 ppm. At this high pH condition, the area corresponding to the

https://doi.org/10.1021/acs.langmuir.3c02181
Langmuir 2023, 39, 15328−15337

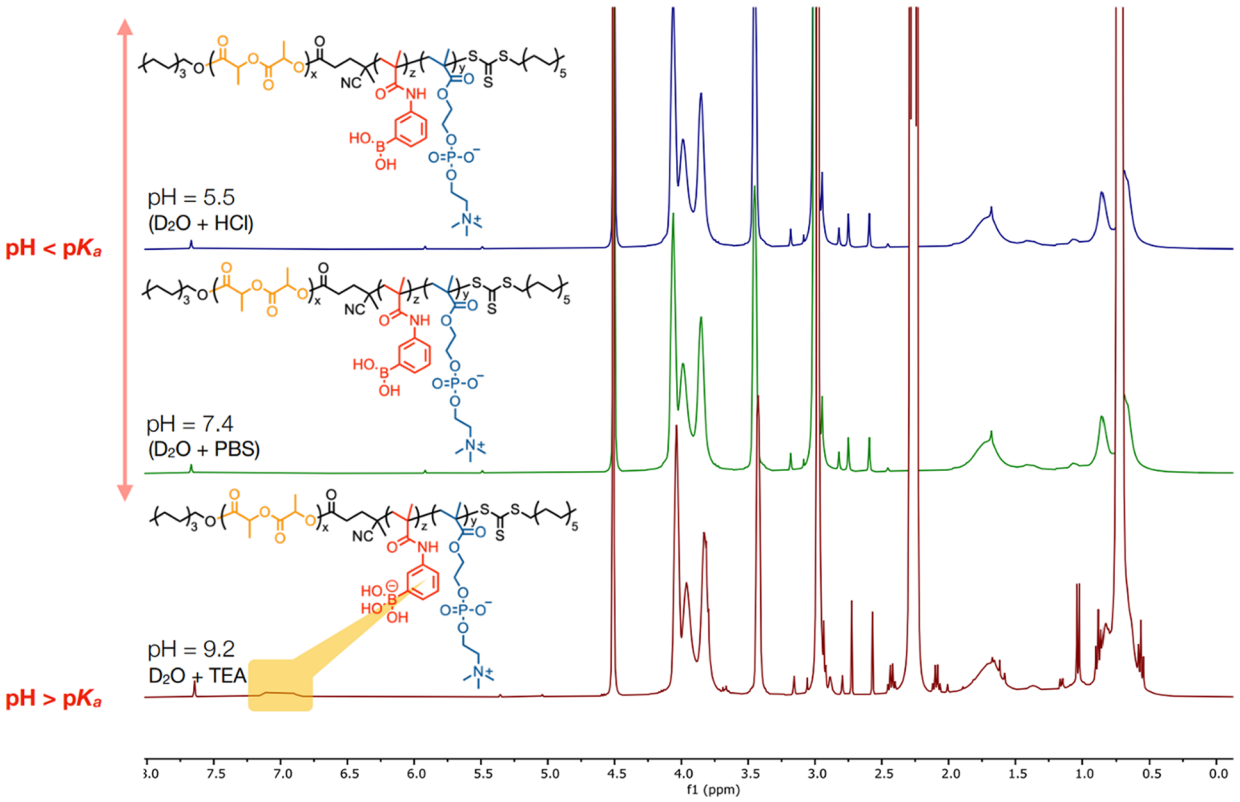

Figure 2. ^{1}H NMR spectra of ZMB3 nanoparticles at pH values above and below the pK_a of the boronic acid showing the signals characteristic of the interlayer block when it is present in the anionic form.

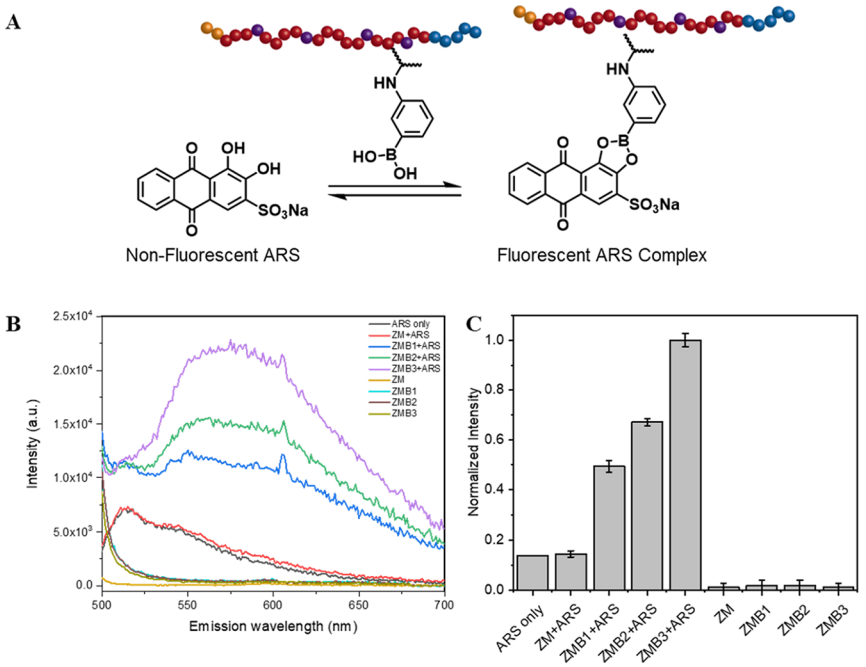

Figure 3. Binding studies of nanoparticles and Alizarin red S (ARS). (A) Schematic of the fluorescent ARS complex. (B) Fluorescence spectra of the complexes formed between ARS (10 μM) and nanoparticles (ZM and ZMB) in PBS. The excitation used was 468 nm. (C) Normalized fluorescence intensity of ARS.

boronic acid signals from ZMB1 nanoparticles corresponded exactly to the value obtained from the polymer in solution (i.e., 8 APMBA repeat units); a slight difference was observed for ZMB2 nanoparticles and ZPB2 polymer, wherein the number of APBMA repeats was 22 and 27, respectively. The greatest difference was for ZPB3, in which case, only 29 of the 47 APMBA repeats were quantified from nanoparticle experiments. The reduced solubility of the PAPBMA block under acidic and neutral pH may be due to limited water diffusion at the boronic acid-rich interlayer given the neutral and

https://doi.org/10.1021/acs.langmuir.3c02181
Langmuir 2023, 39, 15328−15337

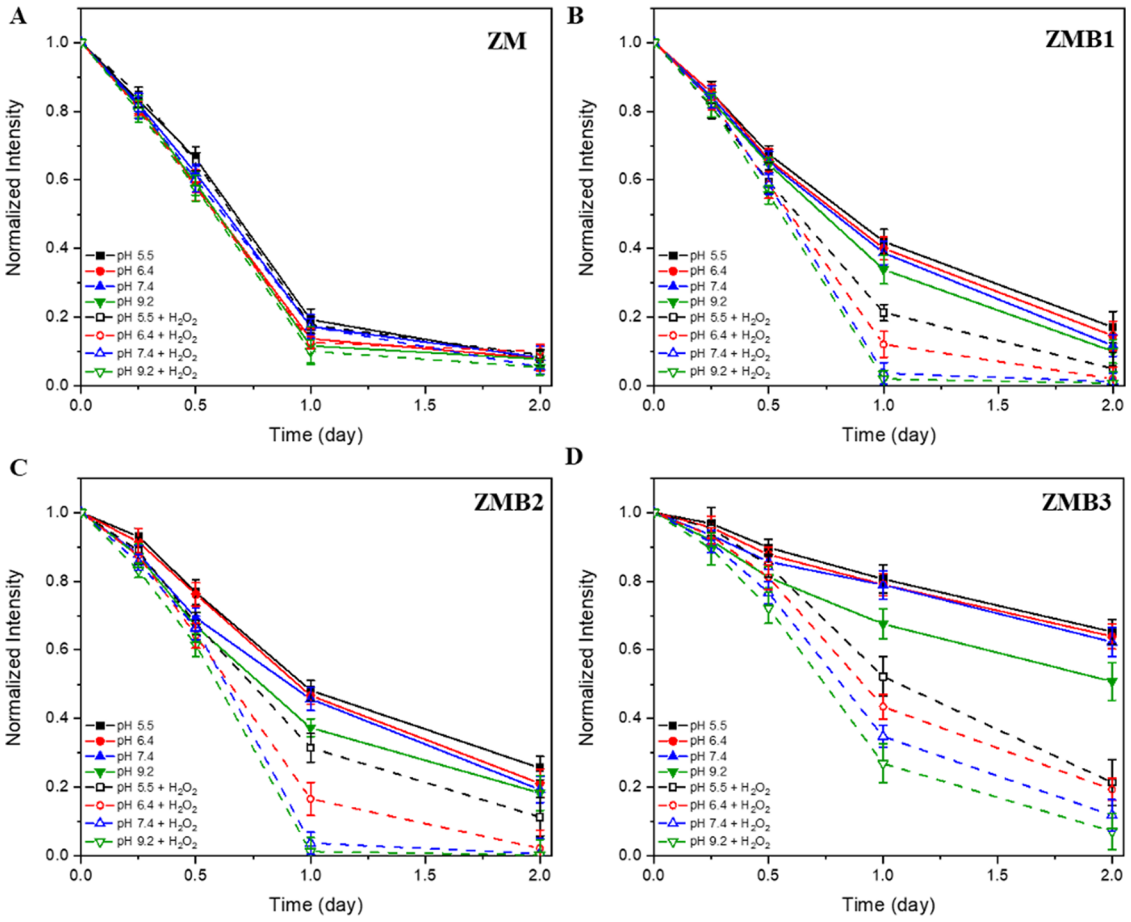

Figure 4. Nile red release kinetic profiles from nanoparticles with increasing PAPBMA block lengths (A–D) at different pH values (solid lines) and in the presence of hydrogen peroxide (dotted lines).

hydrophobic character of the polymer under those conditions, combined with noncovalent associative interactions between boronic acids. These effects would be more important with the PAPBMA block length, as the data show.

The accessibility of boronic acids to the aqueous phase was also examined by Alizarin red S (ARS) binding studies at pH 7.4. ARS is a water-soluble catechol dye, which is non-fluorescent until it complexes with boronic acid; once bound, it fluoresces at an excitation wavelength of 468 nm (Figure 3A). Formation of the boronic ester is particularly favorable, because of the strong interaction between catechols and boronic acids. As shown in Figure 3B, the fluorescence intensity of ARS in a suspension of nanoparticles gradually increases with PAPBMA block length, indicating a higher concentration of boronic acids in the case of nanoparticles from the longest block (ZMB3), in line with the NMR experiment previously discussed. ARS alone and ARS in the presence of nanoparticles from the diblock copolymer ZM, showed a very small signal at 575 nm, whereas no fluorescence was observed for any of the copolymers in the absence of the fluorophore (Figure 3C).

Solute Release Experiments. Nile red was chosen as the hydrophobic solute and loaded into the nanoparticles using the rapid method described above. Solute release was measured over 48 h for nanoparticles from di- and triblock copolymers at pH values above and below the pK_a of APBMA; experiments were run at room temperature and in triplicate. The interaction between Nile red and APBMA was evaluated by ^{11}B and ^{1}H NMR (Figure S10). As there was no shift of the characteristic signals of the monomer in the presence of Nile red, we conclude there is no interaction between the polymer and the solute. Solute release profiles are presented as the filled symbols and solid lines in Figure 4(A–D). As observed, a considerable decrease in the Nile red release rate occurred with increasing PAPBMA block length. For example, after 48 h, nanoparticles from the diblock released 90% of the solute, whereas nanoparticles from triblock copolymers with 8, 27, and 46 APMBA repeats released 85, 73, and 35% of the solute, respectively. A similar trend was observed for shorter times. Additionally, pH was noted to have an effect in modulating the release from APBMA-containing nanoparticles: a higher pH led to faster release. This behavior was more important for nanoparticles from the copolymer with the longest boronic acid block (Figure 4D). The observed differences in release kinetics with the PAPBMA block length and pH also support limited diffusion through the interface due to the combined effects of polymer hydrophobicity and hydrogen bonding. These results are interesting since boronic acids can strongly contribute to solute stabilization even in the absence of binding pairs.

Finally, we investigated the release profile of Nile red-loaded nanoparticles in an oxidative environment. For this, nanoparticles were suspended in an aqueous solution of H_2O_2 (1 mM) and the release was measured over 48 h. The concentration of H_2O_2 used resulted in a H_2O_2:B molar ratio of 147, 49, and 31 for ZMB1, ZMB2, and ZMB3

https://doi.org/10.1021/acs.langmuir.3c02181
Langmuir 2023, 39, 15328–15337

nanoparticles, respectively. The large excess of H_2O_2 used ensured complete oxidation of the PAPBMA block. As shown by the open symbols and dotted lines in Figure 4, the oxidative environment triggered rapid release of the solute from all nanoparticles, except for those assembled from the copolymer without the boronic acid moiety, in which case the oxidant had no effect on the release kinetics. For example, after 48 h at pH 7.4 and in the presence of H_2O_2, the relative amount of Nile red released increased from 88 to 98% for ZMB1, from 81 to 99% for ZMB2, and from 38 to 88% for ZMB3 nanoparticles (Figure 4A−D). This accelerated release can be attributed to two coupled effects. First is the change in the hydrophobicity of the PAPBMA block with oxidation. Comparing the water solubilities of phenylboronic acid (1 g/100 mL) and phenol (8.3 g/100 mL)—the two pendant groups of the PAPBMA block before and after oxidation, respectively—would suggest that the hydrophobicity of the interlayer block decreases with oxidation. This change is dependent on medium pH because of the ionizable character of PAPBMA, such that the difference in water solubility on oxidation would be smaller in more basic environments. The second effect is disruption of the hydrogen-bonded network that occurs with the release of boric acid upon oxidation, eliminating the possibility of hydrogen-bonding at the core−shell interface. Both effects contribute to a solute release behavior similar to that observed for ZMB1 nanoparticles, which lack the functional moiety. The results from Figure 4 also show that release rate increased with pH, consistent with previous reports showing that boronic acid oxidation is more favorable in basic environments.[64,65] Nanoparticle size and size distribution were also tracked by dynamic light scattering experiments during this period and over 7 days, revealing no change regardless of system pH or the presence of the oxidant (Figure S11).

CONCLUSIONS

In conclusion, we successfully developed zwitterionic nanoparticles incorporating a boronic acid-containing middle block through a combination of ROP and RAFT polymerizations. Boronic acid block length was observed to have a direct effect on release kinetics, and nanoparticles from polymers with longer functional blocks showed slower release kinetics compared with nanoparticles from polymers without this moiety. Delayed release was attributed to hydrophobic effects and noncovalent hydrogen bonding associations, which were slightly sensitive to the pH of the environment and strongly influenced by the presence of hydrogen peroxide. In this sense, zwitterionic triblock copolymers incorporating a boronic acid-containing segment can generate pH and H_2O_2 stimuli-responsive nanoparticles even in the absence of binding pairs containing vicinal diols, demonstrating a great potential as target delivery vehicles. Moreover, our results show that the secondary interactions of boronic acids, including hydrophobic effects and hydrogen bonding, should be considered in the design of technologies based on this biologically relevant functionality.

ASSOCIATED CONTENT

Supporting Information

The Supporting Information is available free of charge at https://pubs.acs.org/doi/10.1021/acs.langmuir.3c02181.

^{1}H NMR spectra of all polymers, critical micelle concentration curves, size distribution and transmission electron micrographs of solute-loaded nanoparticles, ^{1}H NMR spectra of nanoparticles, ^{1}H NMR and ^{11}B NMR of APBMA and Nile red, and nanoparticle size at different pH over 7 days (PDF)

AUTHOR INFORMATION

Corresponding Author

Margarita Herrera-Alonso − *Department of Chemical and Biological Engineering and School of Advanced Materials Discovery, Colorado State University, Fort Collins, Colorado 80523, United States;* orcid.org/0000-0002-6064-8699; Email: m.herrera-alonso@colostate.edu

Authors

Jeonghun Lee − *School of Advanced Materials Discovery, Colorado State University, Fort Collins, Colorado 80523, United States;* orcid.org/0000-0002-9996-0110

Karla Cureño Hernandez − *School of Advanced Materials Discovery, Colorado State University, Fort Collins, Colorado 80523, United States*

Sunghoon Kim − *School of Advanced Materials Discovery, Colorado State University, Fort Collins, Colorado 80523, United States*

Complete contact information is available at: https://pubs.acs.org/10.1021/acs.langmuir.3c02181

Notes

The authors declare no competing financial interest.

REFERENCES

(1) Cambre, J. N.; Roy, D.; Gondi, S. R.; Sumerlin, B. S. Facile strategy to well-defined water-soluble boronic acid (co)polymers. *J. Am. Chem. Soc.* **2007**, *129* (34), 10348.

(2) Cheng, F.; Jakle, F. Boron-containing polymers as versatile building blocks for functional nanostructured materials. *Polym. Chem.* **2011**, *2* (10), 2122−2132.

(3) Nishiyabu, R.; Kubo, Y.; James, T. D.; Fossey, J. S. Boronic acid building blocks: tools for self assembly. *Chem. Commun.* **2011**, *47* (4), 1124−1150.

(4) Bull, S. D.; Davidson, M. G.; Van den Elsen, J. M. H.; Fossey, J. S.; Jenkins, A. T. A.; Jiang, Y. B.; Kubo, Y.; Marken, F.; Sakurai, K.; Zhao, J. Z.; James, T. D. Exploiting the Reversible Covalent Bonding of Boronic Acids: Recognition, Sensing, and Assembly. *Acc. Chem. Res.* **2013**, *46* (2), 312−326.

(5) Brooks, W. L. A.; Sumerlin, B. S. Synthesis and Applications of Boronic Acid-Containing Polymers: From Materials to Medicine. *Chem. Rev.* **2016**, *116* (3), 1375−1397.

(6) LeValley, P. J.; Kloxin, A. M. Chemical Approaches to Dynamically Modulate the Properties of Synthetic Matrices. *ACS Macro Lett.* **2019**, *8* (1), 7−16.

(7) Nakahata, M.; Sakai, S. Cross-Linking Building Blocks Using a "Boronate Bridge" to Build Functional Hybrid Materials. *ChemNanoMat* **2019**, *5* (2), 141−151.

(8) Han, G. S.; Domaille, D. W. Connecting the dynamics and reactivity of arylboronic acids to emergent and stimuli-responsive material properties. *J. Mater. Chem. B* **2022**, *10* (33), 6263−6278.

(9) Guan, Y.; Zhang, Y. J. Boronic acid-containing hydrogels: synthesis and their applications. *Chem. Soc. Rev.* **2013**, *42* (20), 8106−8121.

(10) Cash, J. J.; Kubo, T.; Bapat, A. P.; Sumerlin, B. S. Room-Temperature Self-Healing Polymers Based on Dynamic-Covalent Boronic Esters. *Macromolecules* **2015**, *48* (7), 2098−2106.

(11) Deng, C. C.; Brooks, W. L. A.; Abboud, K. A.; Sumerlin, B. S. Boronic Acid-Based Hydrogels Undergo Self-Healing at Neutral and Acidic pH. *ACS Macro Lett.* **2015**, *4* (2), 220−224.

(12) Accardo, J. V.; Kalow, J. A. Reversibly tuning hydrogel stiffness through photocontrolled dynamic covalent crosslinks. *Chem. Sci.* **2018**, *9* (27), 5987−5993.
(13) Smithmyer, M. E.; Deng, C. C.; Cassel, S. E.; LeValley, P. J.; Sumerlin, B. S.; Kloxin, A. M. Self-Healing Boronic Acid-Based Hydrogels for 3D Co-cultures. *ACS Macro Lett.* **2018**, *7* (9), 1105−1110.
(14) Tang, S. C.; Ma, H.; Tu, H. C.; Wang, H. R.; Lin, P. C.; Anseth, K. S. Adaptable Fast Relaxing Boronate-Based Hydrogels for Probing Cell-Matrix Interactions. *Adv. Sci.* **2018**, *5* (9), No. 1800638.
(15) Chen, Y. J.; Tan, Z. Z.; Wang, W. D.; Peng, Y. Y.; Narain, R. Injectable, Self-Healing, and Multi-Responsive Hydrogels via Dynamic Covalent Bond Formation between Benzoxaborole and Hydroxyl Groups. *Biomacromolecules* **2019**, *20* (2), 1028−1035.
(16) Cho, S.; Hwang, S. Y.; Oh, D. X.; Park, J. Recent progress in self-healing polymers and hydrogels based on reversible dynamic B-O bonds: boronic/boronate esters, borax, and benzoxaborole. *J. Mater. Chem. A* **2021**, *9* (26), 14630.
(17) Xu, J. K.; Li, Z.; Fan, Q. Q.; Lv, J.; Li, Y. W.; Cheng, Y. Y. Dynamic Polymer Amphiphiles for Efficient Intracellular and In Vivo Protein Delivery. *Adv. Mater.* **2021**, *33* (52), No. 2104355.
(18) Yang, P.; Zhu, F.; Zhang, Z. B.; Cheng, Y. Y.; Wang, Z.; Li, Y. W. Stimuli-responsive polydopamine-based smart materials. *Chem. Soc. Rev.* **2021**, *50* (14), 8319−8343.
(19) Iturmendi, A.; Monkowius, U.; Teasdale, I. Oxidation Responsive Polymers with a Triggered Degradation via Arylboronate Self-Immolative Motifs on a Polyphosphazene Backbone. *ACS Macro Lett.* **2017**, *6* (2), 150−154.
(20) Qiu, F. Y.; Zhang, M.; Du, F. S.; Li, Z. C. Oxidation Degradable Aliphatic Polycarbonates with Pendent Phenylboronic Ester. *Macromolecules* **2017**, *50* (1), 23−34.
(21) Noh, J.; Jung, E.; Lee, J.; Hyun, H.; Hong, S.; Lee, D. Engineered Polymeric Micelles for Combinational Oxidation Anticancer Therapy through Concurrent HO-1 Inhibition and ROS Generation. *Biomacromolecules* **2019**, *20* (2), 1109−1117.
(22) Jung, E.; Lee, J.; Lee, Y.; Seon, S.; Park, M.; Song, C.; Lee, D. Tumor-Targeting H2O2-Responsive Photosensitizing Nanoparticles with Antiangiogenic and Immunogenic Activities for Maximizing Anticancer Efficacy of Phototherapy. *ACS Appl. Bio Mater.* **2021**, *4* (5), 4450−4461.
(23) Aguirre-Chagala, Y. E.; Santos, J. L.; Aguilar-Castillo, B. A.; Herrera-Alonso, M. Synthesis of Copolymers from Phenylboronic Acid-Installed Cyclic Carbonates. *ACS Macro Lett.* **2014**, *3* (4), 353−358.
(24) Aguirre-Chagala, Y. E.; Santos, J. L.; Huang, Y. X.; Herrera-Alonso, M. Phenylboronic Acid-Installed Polycarbonates for the pH-Dependent Release of Diol-Containing Molecules. *ACS Macro Lett.* **2014**, *3* (12), 1249−1253.
(25) Otsuka, H.; Uchimura, E.; Koshino, H.; Okano, T.; Kataoka, K. Anomalous binding profile of phenylboronic acid with N-acetylneuraminic acid (Neu5Ac) in aqueous solution with varying pH. *J. Am. Chem. Soc.* **2003**, *125* (12), 3493−3502.
(26) Deshayes, S.; Cabral, H.; Ishii, T.; Miura, Y.; Kobayashi, S.; Yamashita, T.; Matsumoto, A.; Miyahara, Y.; Nishiyama, N.; Kataoka, K. Phenylboronic Acid-Installed Polymeric Micelles for Targeting Sialylated Epitopes in Solid Tumors. *J. Am. Chem. Soc.* **2013**, *135* (41), 15501−15507.
(27) Khanal, M.; Vausselin, T.; Barras, A.; Bande, O.; Turcheniuk, K.; Benazza, M.; Zaitsev, V.; Teodorescu, C. M.; Boukherroub, R.; Siriwardena, A.; Dubuisson, J.; Szunerits, S. Phenylboronic-Acid-Modified Nanoparticles: Potential Antiviral Therapeutics. *ACS Appl. Mater. Interfaces* **2013**, *5* (23), 12488−12498.
(28) Tsuchido, Y.; Horiuchi, R.; Hashimoto, T.; Ishihara, K.; Kanzawa, N.; Hayashita, T. Rapid and Selective Discrimination of Gram-Positive and Gram-Negative Bacteria by Boronic Acid-Modified Poly(amidoamine) Dendrimer. *Anal. Chem.* **2019**, *91* (6), 3929−3935.
(29) Khan, T.; Igarashi, K.; Tanabe, A.; Miyazawa, T.; Fukushima, S.; Miura, Y.; Matsumoto, Y.; Yamasoba, T.; Matsumoto, A.; Cabral, H.; Kataoka, K. Structural Control of Boronic Acid Ligands Enhances Intratumoral Targeting of Sialic Acid To Eradicate Cancer Stem-like Cells. *ACS Appl. Bio Mater.* **2020**, *3* (8), 5030−5039.
(30) Miyazaki, T.; Khan, T.; Tachihara, Y.; Itoh, M.; Miyazawa, T.; Suganami, T.; Miyahara, Y.; Cabral, H.; Matsumoto, A. Boronic Acid Ligands Can Target Multiple Subpopulations of Pancreatic Cancer Stem Cells via pH-Dependent Glycan-Terminal Sialic Acid Recognition. *ACS Appl. Bio Mater.* **2021**, *4* (9), 6647−6651.
(31) Bapat, A. P.; Roy, D.; Ray, J. G.; Savin, D. A.; Sumerlin, B. S. Dynamic-Covalent Macromolecular Stars with Boronic Ester Linkages. *J. Am. Chem. Soc.* **2011**, *133* (49), 19832−19838.
(32) Chen, W. X.; Cheng, Y. F.; Wang, B. H. Dual-Responsive Boronate Crosslinked Micelles for Targeted Drug Delivery. *Angew. Chem., Int. Ed.* **2012**, *51* (22), 5293−5295.
(33) Zou, J.; Zhang, S. Y.; Shrestha, R.; Seetho, K.; Donley, C. L.; Wooley, K. L. pH-Triggered reversible morphological inversion of orthogonally-addressable poly(3-acrylamidophenylboronic acid)-block-poly(acrylamidoethylamine) micelles and their shell crosslinked nanoparticles. *Polym. Chem.* **2012**, *3* (11), 3146−3156.
(34) Jackson, A. W.; Fulton, D. A. Making polymeric nanoparticles stimuli-responsive with dynamic covalent bonds. *Polym. Chem.* **2013**, *4* (1), 31−45.
(35) Liu, G.; Ma, R. J.; Ren, J.; Li, Z.; Zhang, H. X.; Zhang, Z. K.; An, Y. L.; Shi, L. Q. A glucose-responsive complex polymeric micelle enabling repeated on-off release and insulin protection. *Soft Matter* **2013**, *9* (5), 1636−1644.
(36) Ren, J.; Zhang, Y. X.; Zhang, J.; Gao, H. J.; Liu, G.; Ma, R. J.; An, Y. L.; Kong, D. L.; Shi, L. Q. pH/Sugar Dual Responsive Core-Cross-Linked PIC Micelles for Enhanced Intracellular Protein Delivery. *Biomacromolecules* **2013**, *14* (10), 3434−3443.
(37) Zhao, Z. W.; Yao, X. M.; Zhang, Z.; Chen, L.; He, C. L.; Chen, X. S. Boronic Acid Shell-Crosslinked Dextran-b-PLA Micelles for Acid-Responsive Drug Delivery. *Macromol. Biosci.* **2014**, *14* (11), 1609−1618.
(38) Butun, V.; Billingham, N. C.; Armes, S. P. Synthesis of shell cross-linked micelles with tunable hydrophilic/hydrophobic cores. *J. Am. Chem. Soc.* **1998**, *120* (46), 12135−12136.
(39) Butun, V.; Lowe, A. B.; Billingham, N. C.; Armes, S. P. Synthesis of zwitterionic shell cross-linked micelles. *J. Am. Chem. Soc.* **1999**, *121* (17), 4288−4289.
(40) Zhang, Q.; Remsen, E. E.; Wooley, K. L. Shell cross-linked nanoparticles containing hydrolytically degradable, crystalline core domains. *J. Am. Chem. Soc.* **2000**, *122* (15), 3642−3651.
(41) Fujii, S.; Cai, Y. L.; Weaver, J. V. M.; Armes, S. P. Syntheses of shell cross-linked micelles using acidic ABC triblock copolymers and their application as pH-responsive particulate emulsifiers. *J. Am. Chem. Soc.* **2005**, *127* (20), 7304−7305.
(42) Read, E. S.; Armes, S. P. Recent advances in shell cross-linked micelles. *Chem. Commun.* **2007**, *29*, 3021−3035.
(43) Elsabahy, M.; Zhang, S. Y.; Zhang, F. W.; Deng, Z. J.; Lim, Y. H.; Wang, H.; Parsamian, P.; Hammond, P. T.; Wooley, K. L. Surface Charges and Shell Crosslinks Each Play Significant Roles in Mediating Degradation, Biofouling, Cytotoxicity and Immunotoxicity for Polyphosphoester-based Nanoparticles. *Sci. Rep.* **2013**, *3*, 3313 DOI: 10.1038/srep03313.
(44) Zhang, F. W.; Elsabahy, M.; Zhang, S. Y.; Lin, L. Y.; Zou, J.; Wooley, K. L. Shell crosslinked knedel-like nanoparticles for delivery of cisplatin: effects of crosslinking. *Nanoscale* **2013**, *5* (8), 3220−3225.
(45) Li, Y. P.; Xiao, W. W.; Xiao, K.; Berti, L.; Luo, J. T.; Tseng, H. P.; Fung, G.; Lam, K. S. Well-Defined, Reversible Boronate Crosslinked Nanocarriers for Targeted Drug Delivery in Response to Acidic pH Values and cis-Diols. *Angew. Chem., Int. Ed.* **2012**, *51* (12), 2864−2869.
(46) Yoshinaga, N.; Ishii, T.; Naito, M.; Endo, T.; Uchida, S.; Cabral, H.; Osada, K.; Kataoka, K. Polyplex Micelles with Phenylboronate/Gluconamide Cross-Linking in the Core Exerting Promoted Gene Transfection through Spatiotemporal Responsivity to Intra-

cellular pH and ATP Concentration. *J. Am. Chem. Soc.* **2017**, *139* (51), 18567−18575.
(47) Liu, H. Y.; Qiao, Z.; Mao, X. X.; Zha, J. C.; Yin, J. Phenylboronic Acid-Dopamine Dynamic Covalent Bond Involved Dual-Responsive Polymeric Complex: Construction and Anticancer Investigation. *Langmuir* **2019**, *35* (36), 11850−11858.
(48) Rodriguez-Cuamatzi, P.; Luna-Garcia, R.; Torres-Huerta, A.; Bernal-Uruchurtu, M. I.; Barba, V.; Hopfl, H. On the Organizing Role of Water Molecules in the Assembly of Boronic Acids and 4,4′-Bipyridine: 1D, 2D and 3D Hydrogen-Bonded Architectures Containing Cyclophane-Type Motifs. *Cryst. Growth Des.* **2009**, *9* (3), 1575−1583.
(49) Ajami, D.; Dube, H.; Rebek, J. Boronic Acid Hydrogen Bonding in Encapsulation Complexes. *J. Am. Chem. Soc.* **2011**, *133* (25), 9689−9691.
(50) Tzeli, D.; Petsalakis, I. D.; Theodorakopoulos, G.; Ajami, D.; Rebek, J. Theoretical study of free and encapsulated carboxylic acid and amide dimers. *Int. J. Quantum Chem.* **2013**, *113* (5), 734−739.
(51) Diemoz, K. M.; Franz, A. K. NMR Quantification of Hydrogen-Bond-Activating Effects for Organocatalysts including Boronic Acids. *J. Org. Chem.* **2019**, *84* (3), 1126−1138.
(52) Foran, G. Y.; Harris, K. J.; Brook, M. A.; Macphail, B.; Goward, G. R. Solid State NMR Study of Boron Coordination Environments in Silicone Boronate (SiBA) Polymers. *Macromolecules* **2019**, *52* (3), 1055−1064.
(53) Fournier, J. H.; Maris, T.; Wuest, J. D.; Guo, W. Z.; Galoppini, E. Molecular tectonics. Use of the hydrogen bonding of boronic acids to direct supramolecular construction. *J. Am. Chem. Soc.* **2003**, *125* (4), 1002−1006.
(54) Chen, Q. J.; Hill, M. R.; Brooks, W. L. A.; Zhu, A. Q.; Sumerlin, B. S.; An, Z. S. Boronic Acid Linear Homopolymers as Effective Emulsifiers and Gelators. *ACS Appl. Mater. Interfaces* **2015**, *7* (39), 21668−21672.
(55) Hsiue, G. H.; Lo, C. L.; Cheng, C. H.; Lin, C. P.; Huang, C. K.; Chen, H. H. Preparation and characterization of poly (2-methacryloyloxyethyl phosphorylcholine)-block-poly(D,L-lactide) polymer nanoparticles. *J. Polym. Sci. Pol Chem.* **2007**, *45* (4), 688−698.
(56) Liu, G. Y.; Lv, P.; Chen, C. J.; Hu, X. F.; Ji, J. A. Biocompatible Poly(D,L-lactide)-block-Poly(2-methacryloyloxyethylphosphorylcholine) Micelles for Drug Delivery. *Macromol. Chem. Physic* **2011**, *212* (6), 643−651.
(57) Chambon, P.; Blanazs, A.; Battaglia, G.; Armes, S. P. Facile Synthesis of Methacrylic ABC Triblock Copolymer Vesicles by RAFT Aqueous Dispersion Polymerization. *Macromolecules* **2012**, *45* (12), 5081−5090.
(58) Liu, G. Y.; Liu, X. S.; Wang, S. S.; Chen, C. J.; Ji, J. Biomimetic Polymersomes as Carriers for Hydrophilic Quantum Dots. *Langmuir* **2012**, *28* (1), 557−562.
(59) Viswanathan, P.; Themistou, E.; Ngamkham, K.; Reilly, G. C.; Armes, S. P.; Battaglia, G. Controlling Surface Topology and Functionality of Electrospun Fibers on the Nanoscale using Amphiphilic Block Copolymers To Direct Mesenchymal Progenitor Cell Adhesion. *Biomacromolecules* **2015**, *16* (1), 66−75.
(60) Lin, W.; Ma, G.; Kampf, N.; Yuan, Z.; Chen, S. Development of Long-Circulating Zwitterionic Cross-Linked Micelles for Active-Targeted Drug Delivery. *Biomacromolecules* **2016**, *17* (6), 2010−2018.
(61) Aguilar-Castillo, B. A.; Santos, J. L.; Luo, H. Y.; Aguirre-Chagala, Y. E.; Palacios-Hernandez, T.; Herrera-Alonso, M. Nanoparticle stability in biologically relevant media: influence of polymer architecture. *Soft Matter* **2015**, *11* (37), 7296−7307.
(62) Petroff, M. G.; Garcia, E. A.; Dengler, R. A.; Herrera-Alonso, M.; Bevan, M. A. kT-Scale Interactions and Stability of Colloids with Adsorbed Zwitterionic and Ethylene Oxide Copolymers. *Macromolecules* **2018**, *51* (22), 9156−9164.
(63) Joralemon, M. J.; O'Reilly, R. K.; Hawker, C. J.; Wooley, K. L. Shell Click-crosslinked (SCC) nanoparticles: A new methodology for synthesis and orthogonal functionalization. *J. Am. Chem. Soc.* **2005**, *127* (48), 16892−16899.
(64) Song, C. C.; Ji, R.; Du, F. S.; Liang, D. H.; Li, Z. C. Oxidation-Accelerated Hydrolysis of the Ortho Ester-Containing Acid-Labile Polymers. *ACS Macro Lett.* **2013**, *2* (3), 273−277.
(65) Garcia, E. A.; Pessoa, D.; Herrera-Alonso, M. Oxidative instability of boronic acid-installed polycarbonate nanoparticles. *Soft Matter* **2020**, *16* (10), 2473−2479.

https://doi.org/10.1021/acs.langmuir.3c02181
Langmuir 2023, 39, 15328−15337